

involve

a journal of mathematics

Qualitative investigation of cytolytic and noncytolytic immune
response in an HBV model

John G. Alford and Stephen A. McCoy



Qualitative investigation of cytolytic and noncytolytic immune response in an HBV model

John G. Alford and Stephen A. McCoy

(Communicated by Martin J. Bohner)

We investigate a mathematical model of infection by the hepatitis B virus (HBV) that includes cytolytic and noncytolytic immune response. The model exhibits a variety of steady-state solutions depending on parameter values, including nonunique and unique equilibrium solutions and periodic behavior. The disease-free equilibrium E_f and the positive-disease equilibrium E_d are examined. The basic reproduction ratio R_0 is computed in order to examine the uniqueness and local asymptotic stability of equilibria and to understand the model's biological implications for HBV dynamics.

1. Introduction

Hepatitis B virus (HBV) is a virus that negatively impacts hundreds of millions of people worldwide by causing chronic infections [Locarnini et al. 2015] in liver cells (or hepatocytes) which may result in scarring of liver tissue and ultimately liver cancer [Lavanchy 2004]. While advances in treatment have resulted in the control or eradication of many infectious diseases, from 1993 to 2013 the rates of death and disability caused by hepatitis rose by 63% and 34%, respectively [Stanaway et al. 2016]. This makes HBV a vital public health concern across the world. Mathematical models are often used to investigate the dynamics of biological phenomena, and virology is an area of study that has been greatly impacted by these models. For example, human immunodeficiency virus (HIV) was thought to replicate at a slow rate, but applications of mathematical models suggested that HIV-1 is in fact a rapidly reproducing virus. This was confirmed by experimental observations [Perelson 2002].

MSC2010: 92C60.

Keywords: mathematical model, hepatitis B viral dynamics, immune response.

The first mathematical model of HBV is discussed in [Nowak et al. 1996] and is given by

$$x' = \lambda - dx - bvx, \quad (1-1a)$$

$$y' = bvx - ay, \quad (1-1b)$$

$$v' = ky - uv, \quad (1-1c)$$

where x is the density of uninfected cells, y is the density of infected cells, and v is the number of free virus cells. Uninfected cells are assumed to be produced at a rate, λ , which may be constant or depend on the total population size of uninfected and infected cells. Uninfected cells die at rate d , and move to the infected class at rate bv , where b is the rate constant describing the infection process. Infected cells die at rate a . Free virions are produced from infected cells at rate k and are removed at rate u .

Many models of HBV have subsequently been investigated including [Rodriguez et al. 2017; Ciupe et al. 2007; Kim et al. 2012; Pang et al. 2012; Hews et al. 2010]. All of these models include variables that specify the density of healthy and unhealthy hepatocytes as well as the density of viral cells in the liver. The dynamics for the immune response is included in [Rodriguez et al. 2017; Ciupe et al. 2007; Kim et al. 2012; Pang et al. 2012]. In general, immune response includes cytolytic (direct killing) and noncytolytic activities. Noncytolytic immune responses use chemical signaling via cytokines to stop the reproduction of HBV within the cell, “curing” the cell without having to destroy it [Vargas-De-León 2014]. Since it is the host’s response to the viral infection and not an innate part of the HBV life cycle that causes hepatocyte destruction (as HBV is not pathological), the role of the noncytolytic immune response is important. In [Wodarza et al. 2002] it was found that if the virus replicates at a fast rate relative to the rate of viral cytopathicity, then a combination of both cytolytic and noncytolytic immune response is more likely to control the disease. On the other hand, if viral cytopathicity is high relative to the replication rate of the virus then cytolytic and noncytolytic immune responses may resolve the infection independently. Citing chimpanzee studies, the authors in [Ciupe et al. 2007] suggest that the noncytolytic response may be the mechanism that causes an early reduction in the HBV viral load, as this occurs much earlier than any detectable cytolytic immune response, liver T cell infiltration, or liver damage. These authors include a fifth variable in their model to account for a cell population of previously infected cells that are refractory to new infection (because of the continuing effects of a noncytolytic immune response) or a population of infected cells not producing measurable amounts of virus.

In this paper a model of HBV dynamics based on these previous models is formulated and analyzed. Here the dynamics for healthy and unhealthy hepatocytes, the virus cells, and the immune cells are included in the model equations.

While [Ciupe et al. 2007; Kim et al. 2012] are mainly concerned with validating HBV models and investigating HBV dynamics utilizing patient data and computer simulations, in this paper the model equations are mathematically analyzed to determine the reproduction ratio and give conditions that guarantee stability of the disease equilibria, as in [Rodriguez et al. 2017; Pang et al. 2012; Hews et al. 2010]. Unlike [Rodriguez et al. 2017; Hews et al. 2010], the model here includes a fourth equation for the immune response dynamics, and unlike [Pang et al. 2012] the growth dynamics for healthy and unhealthy hepatocytes are logistic. The paper is outlined as follows. In Section 2 the model equations are presented and described. In Section 3 these equations are nondimensionalized and then the disease-free equilibrium is analyzed in Section 4. The disease equilibrium is discussed in Section 5 and in Section 6 a reduced system is presented, the disease equilibrium is analyzed, and the main theorems are proven. Finally, these results are summarized and future work is suggested in the conclusion, Section 7.

2. Model equations

The following model for hepatitis B dynamics builds on the basic framework of previous HBV models, including [Rodriguez et al. 2017; Ciupe et al. 2007; Kim et al. 2012; Pang et al. 2012; Hews et al. 2010]. The state variables include healthy hepatocyte density (X), unhealthy hepatocyte density (Y), and number of virus cells (V), just as in (1-1a), (1-1b), and (1-1c). A third variable I is now included to account for the density of immune response cells. The equations are

$$X' = r_1 X \left(1 - \frac{X+Y}{K}\right) - \beta X V + f b Y I, \quad (2-1a)$$

$$Y' = r_2 Y \left(1 - \frac{X+Y}{K}\right) + \beta X V - b Y I, \quad (2-1b)$$

$$V' = \gamma Y - \mu V, \quad (2-1c)$$

$$I' = c Y - d I + I_0. \quad (2-1d)$$

Here both the healthy hepatocyte cell population dynamics (2-1a) and the unhealthy hepatocyte cell population dynamics (2-1b) are maintained by homeostasis as they are governed by logistic dynamics, as in [Rodriguez et al. 2017; Ciupe et al. 2007]. That is, the first terms in (2-1a) and (2-1b) yield negative per-capita growth rates when $X + Y > K$, where $K > 0$ is a parameter that defines hepatocyte carrying capacity. Healthy hepatocytes and infected hepatocytes proliferate at rates $r_1 > 0$ and $r_2 > 0$. Here it will be assumed that $r_1 \geq r_2$ as in [Rodriguez et al. 2017] so that healthy cells proliferate at least as fast as unhealthy cells. The parameter $\beta > 0$ controls the rate at which healthy hepatocytes are infected by virions so that the rate of infection is directly proportional to β and the density of healthy hepatocytes

(i.e., mass action), just as in [Rodriguez et al. 2017; Ciupe et al. 2007; Kim et al. 2012; Pang et al. 2012]. The last terms in (2-1a) and (2-1b) represent the immune response to disease. The parameter $b > 0$ controls the cytolytic clearance rate of infected cells and the noncytolytic “curing” of infected cells, given by the last term in (2-1a), includes a scaling parameter f . Here $f \in (0, 1]$ as in [Kim et al. 2012], where the authors refer to f as a “calibration coefficient”.

The viral dynamics (2-1c) and immune response dynamics (2-1d) are linear. The parameters $\gamma > 0$ and $c > 0$ control the rates at which virions and immune cells are produced in response to the number of unhealthy hepatocytes respectively. Thus $1/\mu$ and $1/d$ specify the average lifetime of a free virus particle [Nowak and Bangham 1996] and an immune cell [Ciupe et al. 2007] respectively. In the absence of unhealthy hepatocytes, immune cells grow at a constant rate I_0 , as in [Ciupe et al. 2007; Kim et al. 2012; Pang et al. 2012], and the ratio I_0/d quantifies the basal level of immune cells [Ciupe et al. 2007] in the body.

The model presented here is distinct from the various models that have been studied previously. For example, in [Nowak et al. 1996; Kim et al. 2012; Pang et al. 2012], healthy hepatocytes (in the absence of immune response) grow at a constant rate. In [Nowak et al. 1996; Pang et al. 2012; Hews et al. 2010] unhealthy hepatocyte growth occurs only by infection of healthy cells. While the investigators in [Kim et al. 2012] allow for growth of unhealthy hepatocytes in the absence of infection, the growth dynamics is linear (proportional to the density of unhealthy cells) rather than logistic.

Example parameter values determined from patient data can be found in the literature. Table 1 displays typical values or ranges of values from [Rodriguez et al.

parameter	description	value	ref.
r_1	healthy-cell proliferation rate	(0,4] day ⁻¹	R
r_2	unhealthy-cell proliferation rate	(0,4] day ⁻¹	R
K	carrying capacity	1.9×10^7 mL ⁻¹	R
β	healthy-cell infection rate	$(10^{-10}, 10^{-6})$ mL day ⁻¹	R
f	noncytolytic scaling parameter	(0, 1]	K
b	cytolytic clearance rate	7×10^{-4} mL day ⁻¹	K
γ	viral production rate	[1.4,164] day ⁻¹	K
μ	viral clearance rate	[0.18, 1] day ⁻¹	R
c	CTL response rate	0.5 day ⁻¹	K
d	CTL death rate	0.5 day ⁻¹	K
I_0	CTL production rate	9.33 mL ⁻¹ day ⁻¹	K

Table 1. Example parameter values. Here R stands for [Rodriguez et al. 2017] and K for [Kim et al. 2012].

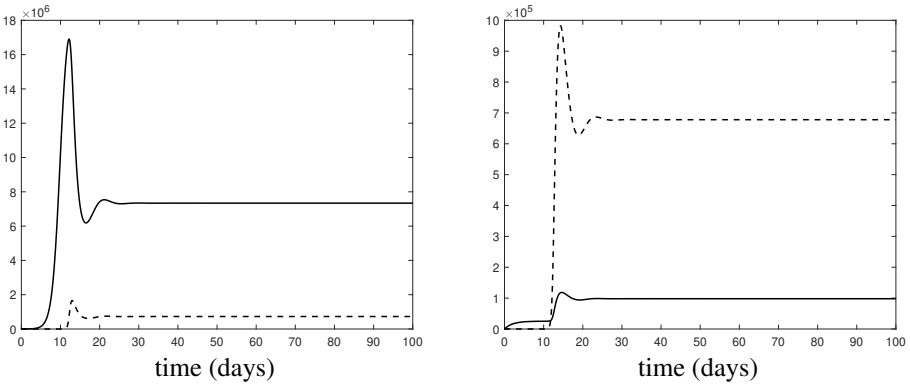


Figure 1. Simulation of (2-1a)–(2-1d). The left panel shows X (solid) and Y (dashed), where Y has been scaled by a factor of 10. The right panel shows I (solid) and V (dashed). Here $r_1 = 1$, $r_2 = 0.5$, $\beta = 10^{-6}$, $f = 0.1$, $\gamma = 6.24$, $\mu = 0.67$ and the remaining parameters are as in Table 1.

2017; Kim et al. 2012]. The last column displays the reference. The units assume that X , Y , and I are measured as the number of cells per mL, and V is measured as number of virions.

Simulations of (2-1a)–(2-1d) are shown in Figures 1 and 2. In each case, the initial conditions are that $X(0) = 1000$, $Y(0) = 100$, $V(0) = 10$, and $I(0) = 0$. Figure 2 illustrates that if the cytolytic clearance rate b is much smaller than the value listed in Table 1, the model exhibits periodic solutions as in [Hews et al. 2010].

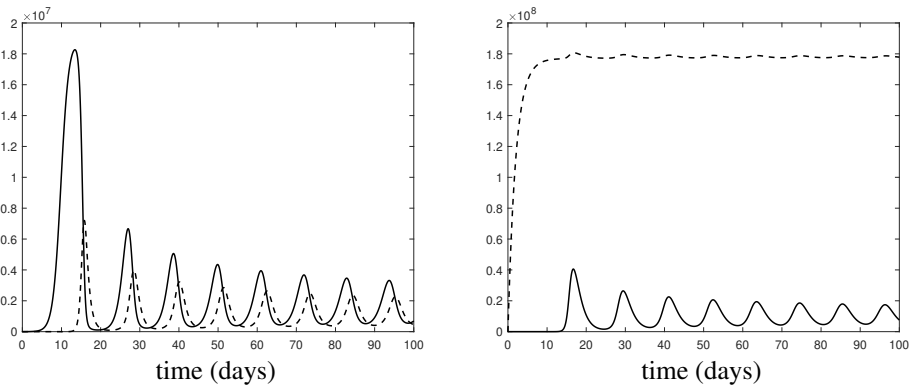


Figure 2. Simulation of (2-1a)–(2-1d). The left panel shows X (solid) and Y (dashed) and the right panel shows I (solid) and V (dashed). Here $b = 10^{-8}$, $r_1 = 1$, $r_2 = 0.5$, $\beta = 10^{-7}$, $f = 0.1$, $\gamma = 6.24$, $\mu = 0.67$ and the remaining parameters are as in Table 1.

3. Nondimensional equations

In order to analyze the steady-state solutions, it will be useful to nondimensionalize the model equations (2-1a)–(2-1d). The nondimensional parameters that will be used are

$$\hat{t} := r_2 t, \quad \hat{x} := \frac{X}{K}, \quad \hat{y} := \frac{Y}{K}, \quad \hat{v} := \left(\frac{\beta}{r_2}\right)V, \quad \hat{\alpha} := \frac{I}{K}.$$

After substituting these into (2-1a)–(2-1d) the system is transformed into

$$\hat{x}' = r\hat{x}(1 - \hat{x} - \hat{y}) - \hat{x}\hat{v} + f\varphi\hat{y}\hat{\alpha}, \tag{3-1a}$$

$$\hat{y}' = \hat{y}(1 - \hat{x} - \hat{y}) + \hat{x}\hat{v} - \varphi\hat{y}\hat{\alpha}, \tag{3-1b}$$

$$\hat{v}' = p_1\hat{y} - q_1\hat{v}, \tag{3-1c}$$

$$\hat{\alpha}' = p_2\hat{y} - q_2\hat{\alpha} + I_0 r_2 K, \tag{3-1d}$$

where

$$\varphi := bKr_2, \quad p_1 := K\gamma\beta r_2^2, \quad p_2 := cr_2, \quad q_1 := \mu r_2, \quad q_2 := dr_2. \tag{3-2}$$

Next we define

$$\omega := I_0 d K \tag{3-3}$$

and substitute $\alpha = \hat{\alpha} - \omega$ in (3-1a)–(3-1d) to get the homogeneous system

$$x' = rx(1 - x - y) - xv + f\varphi y(\alpha + \omega), \tag{3-4a}$$

$$y' = y(1 - x - y) + xv - \varphi y(\alpha + \omega), \tag{3-4b}$$

$$v' = p_1 y - q_1 v, \tag{3-4c}$$

$$\alpha' = p_2 y - q_2 \alpha. \tag{3-4d}$$

If the right side of each equation (3-4a)–(3-4d) is denoted by $F_j(x_1, x_2, x_3, x_4)$, with $j = 1, 2, 3, 4$ and $x_1 = x, x_2 = y, x_3 = v$, and $x_4 = \alpha$, the system clearly satisfies $F_k(x_1, x_2, x_3, x_4) \geq 0$ whenever $x_k = 0$ and $x_j \in [0, \infty), k \neq j$. This implies solutions are nonnegative for nonnegative initial data [Thieme 2003]. The long-term behavior of the system is governed by any stable steady-states that may exist, so it is essential to understand how these solutions arise. Here only the constant steady-states (or equilibria) will be analyzed. In fact, this system has multiple equilibria. The trivial equilibrium is $E_0 = (0, 0, 0, 0)$ and the disease-free equilibrium is $E_f = (1, 0, 0, 0)$. The disease equilibrium will be denoted by $E_d = (x^*, y^*, v^*, \alpha^*)$, where $x^*, y^*, v^*, \alpha^* > 0$ since this is the sustained infection case. In the following sections the existence, uniqueness, and stability properties will be investigated for E_f and E_d . The trivial equilibrium is not considered as it represents total death of all hepatocytes. Furthermore, the equilibrium $(0, y^*, v^*, \alpha^*)$ will not be considered as it represents death of all healthy hepatocytes.

4. Disease-free equilibrium

The Jacobian of (3-4a)–(3-4d) is the matrix

$$J(x, y, v, \alpha) = \begin{bmatrix} r(1-2x-y)-v & -rx+f\varphi(\alpha+\omega) & -x & f\varphi y \\ -y+v & 1-x-2y-\varphi(\alpha+\omega) & x & -\varphi y \\ 0 & p_1 & -q_1 & 0 \\ 0 & p_2 & 0 & -q_2 \end{bmatrix}. \quad (4-1)$$

Substituting E_f into (4-1) yields the matrix

$$J(1, 0, 0, 0) = \begin{bmatrix} -r & -r+f\varphi\omega & -1 & 0 \\ 0 & -\varphi\omega & 1 & 0 \\ 0 & p_1 & -q_1 & 0 \\ 0 & p_2 & 0 & -q_2 \end{bmatrix}, \quad (4-2)$$

which results in the following characteristic equation for the eigenvalue λ :

$$p(\lambda) = (r + \lambda)(q_2 + \lambda)[\lambda^2 + (q_1 + \varphi\omega)\lambda + \varphi\omega q_1 - p_1]. \quad (4-3)$$

Thus two eigenvalues are $\lambda = -r < 0$ and $\lambda = -q_2 < 0$, while the remaining two are

$$\lambda = -(q_1 + \varphi\omega) \pm \sqrt{(q_1 - \varphi\omega)^2 + 4p_1 2}.$$

It follows that all eigenvalues are real. Furthermore, since

$$(q_1 - \varphi\omega)^2 + 4p_1 = (q_1 + \varphi\omega)^2 - 4(\varphi\omega q_1 - p_1),$$

each eigenvalue is negative if and only if $\varphi\omega q_1 - p_1 > 0$. It follows from [Thieme 2003; Allen 2007] that a necessary and sufficient condition for the disease-free equilibrium to be locally asymptotically stable is that $p_1/(\varphi\omega q_1) < 1$. This yields the *basic reproduction ratio*, denoted by R_0 , defined by

$$R_0 := p_1\varphi\omega q_1. \quad (4-4)$$

This ratio measures the average number of newly infected cells generated from one infected cell at the beginning of the infectious process [Wodarza et al. 2002; Pang et al. 2012; Thieme 2003]. Typically, for infectious disease models the basic reproduction ratio specifies a parameter grouping that provides a threshold [Diekmann et al. 1990] for infection to occur. That is, the disease will invade if $R_0 > 1$ or will not invade if $R_0 < 1$. Figure 3 shows simulations of healthy- and unhealthy-cell densities for the nondimensionalized equations (3-4a)–(3-4d), which illustrate this threshold behavior. When $R_0 = 0.9$, the steady-state value of healthy-cell density is 1 and the steady-state value of unhealthy-cell density is 0. However, for $R_0 > 1$ the disease state exists and steady-state values for healthy-cell density decrease with R_0 , whereas the steady-state values for unhealthy-cell density increase with R_0 .

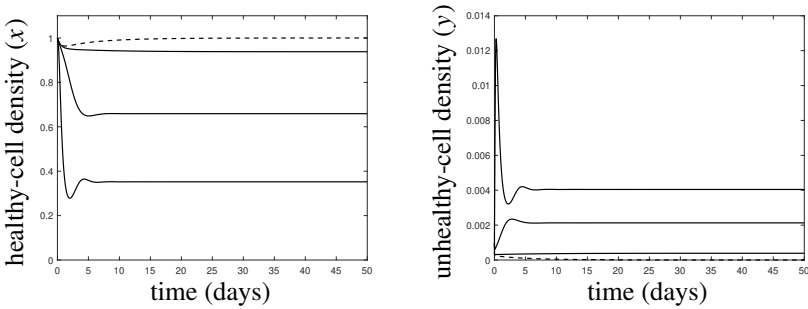


Figure 3. Simulations of (3-4a)–(3-4d) with healthy-cell density (x) on the left and unhealthy-cell density (y) on the right for $R_0 = 0.9$, $R_0 = 1.1$, $R_0 = 2$, and $R_0 = 20$, where R_0 is defined in (4-4). Dashed curves depict $R_0 = 0.9$ and solid curves correspond to values of $R_0 > 1$. The steady-state for $R_0 = 0.9$ is the disease-free equilibrium E_f , while the steady-state for $R_0 > 1$ is the disease equilibrium E_d . As R_0 increases, steady-state values of x decrease, while steady-state values of y increase.

The sections that follow investigate how the disease equilibrium E_d is affected by the parameters in the model. Section 5 establishes parameter ranges that guarantee uniqueness of E_d . In Section 6, parameter ranges are determined that guarantee the local asymptotic stability of E_d in a reduced model.

5. Disease equilibrium

In this section, the disease equilibrium $E_d = (x^*, y^*, v^*, \alpha^*)$ is computed and its parameter-dependence is investigated numerically. Assuming x^*, y^*, v^*, α^* are positive constants, then using (3-4b)–(3-4d) these constants satisfy

$$y^* = 1\theta(1 - \varphi\omega - \rho x^*), \quad v^* = \frac{p_1}{q_1}y^*, \quad \alpha^* = p_2q_2y^*, \tag{5-1}$$

where

$$\theta := 1 + p_2q_2\varphi, \quad \rho := 1 - \frac{p_1}{q_1}. \tag{5-2}$$

Substituting these values in (3-4a) results in the quadratic equation for the healthy-cell density $\kappa_2x^2 + \kappa_1x + \kappa_0 = 0$, where

$$\kappa_2 := -\rho\left(r\lambda - \frac{p_1}{\theta q_1}\right) - r\frac{p_1}{q_1} + \frac{f}{\theta}\lambda\rho^2, \tag{5-3a}$$

$$\kappa_1 := (1 - \varphi\omega)\left(r\lambda - \frac{p_1}{\theta q_1}\right) + r\varphi\omega - f\frac{\rho}{\theta}[\varphi\omega + 2\lambda(1 - \varphi\omega)], \tag{5-3b}$$

$$\kappa_0 := \frac{f}{\theta}\{\lambda(1 - \varphi\omega)^2 + \varphi\omega(1 - \varphi\omega)\}, \tag{5-3c}$$

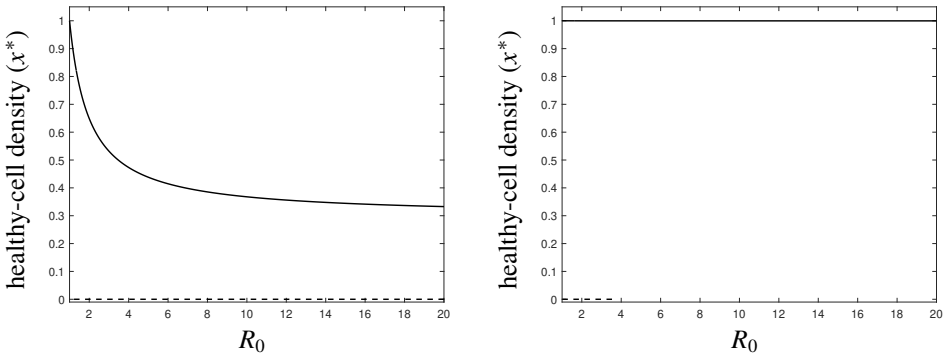


Figure 4. The healthy-cell density computed from (5-5) for the disease equilibrium E_d plotted as a function of $1 < R_0 < 20$. Here ω is varied, while all other parameters are fixed and R_0 is computed from (4-4). The healthy-cell infection rates are $\beta = 10^{-6}$ mL day $^{-1}$ (left) and $\beta = 10^{-8}$ mL day $^{-1}$ (right). In both panels the remaining parameter values are as in Table 1, with $r_1 = 1$, $r_2 = 0.5$, $f = 0.01$, $\gamma = 6.24$, and $\mu = 0.67$. Solid curves are stable positive equilibria, while dashed curves (near zero) are unstable positive equilibria.

with λ defined as

$$\lambda := \varphi p_2 \theta q_2 = \varphi p_2 \varphi p_2 + q_2. \tag{5-4}$$

The healthy-cell density for the disease equilibrium is then

$$x^* = -12\kappa_2 [\kappa_1 \pm \sqrt{\kappa_1^2 - 4\kappa_2\kappa_0}], \tag{5-5}$$

where κ_i ($i = 0, 1, 2$) are given by (5-3a)–(5-3c). The remaining values for the disease equilibrium are then easily computed from (5-1). After some algebra, we get from (5-3a), (5-3b), and (5-3c) that

$$\begin{aligned} \kappa_1^2 - 4\kappa_2\kappa_0 = & \left[(1-\varphi\omega) \left(r\lambda - \theta^{-1} \frac{p_1}{q_1} \right) + r\varphi\omega + \rho\varphi\omega f\theta^{-1} \right]^2 \\ & + 4r\varphi\omega f\theta^{-1} (R_0 - 1) [\varphi\omega(1-\lambda) + \lambda], \end{aligned} \tag{5-6}$$

$$\kappa_2 = -r \left\{ \frac{p_1}{q_1} + \lambda\rho \right\} + \theta^{-1} \rho \left\{ \frac{p_1}{q_1} + \lambda f\rho \right\}, \tag{5-7}$$

$$\kappa_2 + \kappa_1 + \kappa_0 = \varphi\omega r (R_0 - 1)(\lambda - 1) + (\varphi\omega)^2 \theta^{-1} (R_0 - 1) [f(1-\lambda) - R_0(1-\lambda f)]. \tag{5-8}$$

Note from the definition of R_0 in (4-4) that if all parameters are fixed except ω , then $R_0 \downarrow 1$ if and only if $\omega \uparrow \bar{\omega}$, where

$$\bar{\omega} := p_1 \varphi q_1. \tag{5-9}$$

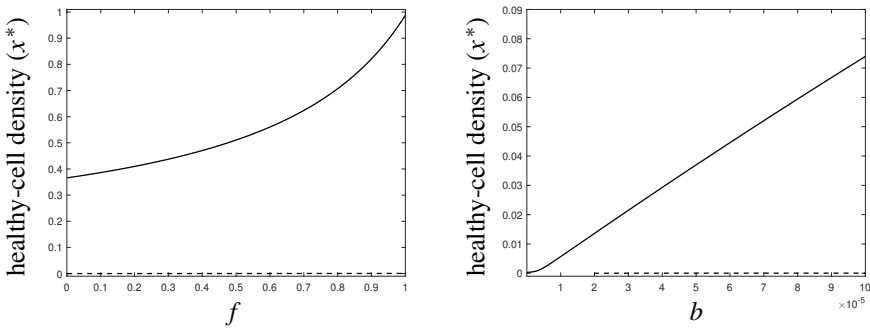


Figure 5. The healthy-cell density computed from (5-5) for the disease equilibrium E_d plotted as a function of noncytolytic scaling $f \in (0, 1]$ (left) and cytolytic clearance rate b (right) when $f = 0.1$. The healthy-cell infection rate is $\beta = 10^{-6}$ mL day $^{-1}$. In both panels $R_0 = 10$ and the remaining parameter values are as in Table 1, with $r_1 = 1$, $r_2 = 0.5$, $\gamma = 6.24$, and $\mu = 0.67$. Solid curves are stable positive equilibria, while dashed curves (near zero) are unstable positive equilibria. Note the difference in vertical scale in each plot.

In this case, $x^* \uparrow 1$, since $\kappa_1 + \kappa_2 + \kappa_0 = 0$ when $R_0 = 1$. Furthermore, $\omega \downarrow 0$ is equivalent to $R_0 \uparrow \infty$ and in this case

$$x^* \downarrow -12\kappa_2 \left[\kappa_1(0) \pm \sqrt{\kappa_1(0)^2 - 4\kappa_2\kappa_0(0)} \right],$$

where $\kappa_0(0)$ and $\kappa_1(0)$ are from (5-3b) and (5-3c) respectively when $\omega = 0$.

Figure 4 shows the density of healthy cells x^* for the disease equilibrium as a function of R_0 when $1 < R_0 < 20$. Here R_0 is determined from ω as in (4-4) with all other parameters fixed. The two plots in the figure represent two different values for the healthy-cell infection rate β . If $\beta = 10^{-6}$ mL day $^{-1}$ (as in the left panel), there are two positive equilibria for each value of R_0 where the smaller is near zero and the larger decreases from a value of 1 to a value of approximately 0.33. If $\beta = 10^{-8}$ mL day $^{-1}$, there is a bifurcation at $R_0 \approx 3.5$ so that two positive equilibria exist for $R_0 < 3.5$ and there is a unique positive equilibrium for $R_0 > 3.5$. In each case, stability was determined from Matlab by computing the eigenvalues of (4-1) evaluated at E_d .

Figures 5 and 6 show the density of healthy cells x^* for the disease equilibrium when $R_0 = 10$ as it depends on both the noncytolytic scaling parameter f and the cytolytic clearance rate b . When healthy-cell infection rate β is relatively large as in Figure 5, the density of healthy cells is much more sensitive to changes in f than b . Conversely, when β is relatively small as in Figure 6, the density of healthy cells is much more sensitive to changes in b than f . The logarithm of x^* is shown

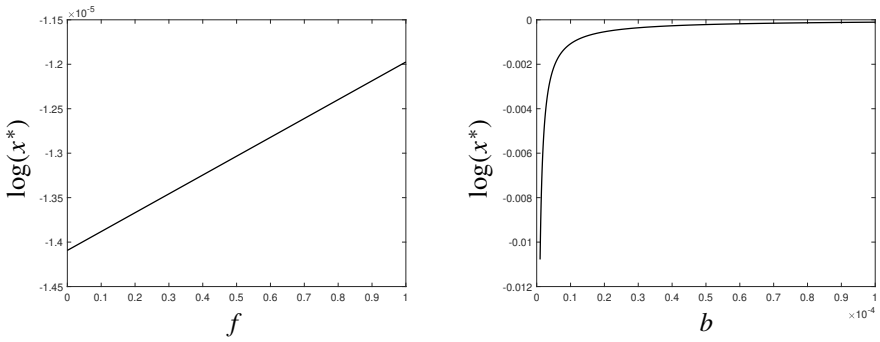


Figure 6. The logarithm (base 10) of the healthy-cell density computed from (5-5) for the disease equilibrium E_d plotted as a function of noncytolytic scaling $f \in (0, 1]$ (left) and cytolytic clearance rate b (right) when $f = 0.1$ and $R_0 = 10$. The healthy-cell infection rate is $\beta = 10^{-9}$ mL day $^{-1}$. In both panels the remaining parameter values are as in Table 1, with $r_1 = 1$, $r_2 = 0.5$, $\gamma = 6.24$, $\mu = 0.67$, $c = d = 0.5$. Here the parameters satisfy the conditions of Theorem 5.1.

in Figure 6 to illustrate that these solutions obey $0 < x^* < 1$. Furthermore, there is a unique value for x^* over all parameter values given in the figure. In Figure 6 the parameter ρ defined in (5-2) is positive and it will next be shown in Theorem 5.1 that this condition is sufficient so that the disease equilibrium is real, bounded, and unique when $R_0 > 1$.

Theorem 5.1. Assume $R_0 > 1$, $\rho > 0$, $0 < f \leq 1$, and $r \geq 1$. Then system (3-4a)–(3-4d) has a unique, positive-disease equilibrium E_d .

Proof. If $R_0 > 1$, then from (5-6) it is clear that $\kappa_1^2 - 4\kappa_2\kappa_0 > 0$ since $0 < \lambda < 1$. From (5-7), the coefficient $\kappa_2 < 0$ if and only if

$$r\theta > \rho \frac{p_1}{q_1} + \lambda f \rho \frac{p_1}{q_1} + \lambda \rho,$$

which follows immediately from the bounds $\theta > 1$, $0 < \lambda < 1$, and the assumptions of the theorem. Using the definition of ρ , φ , and ω from (3-2), (3-3) and (5-2) and the assumption that ρ is positive means that $p_1/q_1 < 1$ and noting that p_1/q_1 is equivalent to $\varphi\omega R_0$, it follows that $\varphi\omega < 1$ and hence $\kappa_0 > 0$. Therefore $\kappa_2 x^2 + \kappa_1 x + \kappa_0$, where κ_i ($i = 0, 1, 2$) are given by (5-3a)–(5-3c), has two real solutions with opposite signs. From (5-8), the sum $\kappa_2 + \kappa_1 + \kappa_0 < 0$ follows easily since $f \leq 1 < R_0$ and $\lambda < 1$. It then follows that the positive root of $\kappa_2 x^2 + \kappa_1 x + \kappa_0$ must be less than 1, and we get $0 < x^* < 1$. In this case, since $R_0 > 1$ is equivalent to $\rho < 1 - \varphi\omega$, inspection of (5-1) shows that $y^* > 0$, $v^* > 0$, and $\alpha^* > 0$. \square

In the following section the local asymptotic stability of the disease equilibrium will be considered using a reduced system. In particular, a system of three equations is presented which mimics x , y , and v from (3-4a), (3-4b), and (3-4c) under certain parameter constraints and allows for a more tractable analytical result.

6. Reduced system

The parameter values in Table 1 have thus far provided baseline values for simulations. There is evidence in the literature that supports the investigation of smaller values for both b (cytolytic clearance rate) and c (CTL response rate). The authors in [Ciupe et al. 2007] conjecture that a patient who was immunosuppressed because of a corticosteroid drug regimen had weak cytotoxic clearance rate and low immune response rate which corresponds to reductions in the values of both b and c . In [Zapata et al. 2014] the ratio of the rate of immune response activation to the death rate of immune response (i.e., c/d in (2-1d)) is given as 0.02, which is much smaller than $c/d = 1$ from Table 1.

Inspection of (3-2) shows that decreasing b corresponds to decreasing φ and decreasing c/d corresponds to decreasing p_2/q_2 . Numerical experimentation shows that as either φ or p_2/q_2 get smaller and smaller from the baseline values that are suggested by Table 1, the values x , y , and v computed from (3-4a)–(3-4d) are better and better approximated by solutions of the reduced system given by

$$x' = rx(1 - x - y) - xv + f\varphi y(\alpha^* + \omega), \tag{6-1a}$$

$$y' = y(1 - x - y) + xv - \varphi y(\alpha^* + \omega), \tag{6-1b}$$

$$v' = p_1y - q_1v, \tag{6-1c}$$

where $\alpha^* = \eta y^*$ with $\eta := p_2/q_2$, which is the equilibrium value for α obtained from (3-4d).

The disease equilibrium (x^*, y^*, v^*) for the reduced system (6-1a)–(6-1c) is equivalent to E_d from Section 5 when α^* is included. Thus, Theorem 5.1 also applies to (6-1a)–(6-1c). The Jacobian evaluated at the disease equilibrium is

$$J(x^*, y^*, v^*) = \begin{bmatrix} t_1 & t_3 & -x^* \\ -\rho y^* & t_2 & x^* \\ 0 & p_1 & -q_1 \end{bmatrix}, \tag{6-2}$$

where

$$t_1 = r(1 - 2x^* - y^*) - (1 - \rho)y^*, \tag{6-3}$$

$$t_2 = 1 - x^* - 2y^* - \varphi(\eta y^* + \omega) = -(1 - \rho)x^* - y^*, \tag{6-4}$$

$$t_3 = -rx^* + f\varphi(\eta y^* + \omega). \tag{6-5}$$

Here t_2 simplifies using $1 - x^* - y^* = \varphi(\alpha^* + \omega) - (1 - \rho)x^*$ from (6-1b). The characteristic equation is cubic $\lambda^3 + a_1\lambda^2 + a_2\lambda + a_3 = 0$, where

$$a_1 = q_1 - t_1 - t_2, \quad (6-6)$$

$$a_2 = t_1 t_2 - q_1(t_1 + t_2) - p_1 x^* + \rho t_3 y^*, \quad (6-7)$$

$$a_3 = q_1 t_1 t_2 + p_1 t_1 x^* + \rho q_1 t_3 y^* - \rho p_1 x^* y^*. \quad (6-8)$$

The Routh–Hurwitz conditions [Edelstein-Keshet 1988] will be used to derive necessary and sufficient conditions so that (x^*, y^*, α^*) is locally asymptotically stable. These conditions are that

$$a_1 > 0, \quad a_3 > 0, \quad a_1 a_2 > a_3. \quad (6-9)$$

Inspection of the dimensional system (2-1a)–(2-1d) shows that the constant cytolytic immune response rate I_0 will affect the steady-states for α . In the nondimensional system, I_0 controls $\omega = I_0/(dK)$ from (3-3). The following analysis uses ω as the main parameter to derive bounds on the other parameters and show that the Routh–Hurwitz conditions hold. Recall that x^* is determined from solutions of the quadratic equation

$$\kappa_2 x^2 + \kappa_1(\omega)x + \kappa_0(\omega) = 0, \quad (6-10)$$

where κ_i ($i = 0, 1, 2$) are given by (5-3a)–(5-3c). Note that the coefficient κ_2 does not depend on ω , while κ_1 and κ_0 both depend on ω , and this has been made explicit in the notation. Therefore, x^* also depends on ω , which will be denoted as $x^*(\omega)$. Assuming the conditions in Theorem 5.1, $0 < x^*(\omega) < 1$ and $x^*(\omega)$ is defined for $\omega \in (0, \bar{\omega})$, where $\bar{\omega}$ is defined in (5-9). Furthermore, (5-3b) shows that κ_1 is a linear function of ω and that

$$\begin{aligned} \kappa_1'(\omega) &= \frac{d\kappa_1}{d\omega} = \varphi \left\{ - \left(r\lambda - \frac{p_1}{\theta q_1} \right) + r - f \frac{\rho}{\theta} [1 - 2\lambda] \right\}, \\ \kappa_1(0) &= r\lambda - \frac{p_1}{\theta q_1} - 2\lambda f \frac{\rho}{\theta}. \end{aligned} \quad (6-11)$$

The following lemma derives a lower bound on $x^*(\omega)$ by replacing $\kappa_0(\omega)$ in (6-10) with a lower bound.

Lemma 6.1. *Assume all parameters are fixed except ω . Suppose that $R_0 > 1$, $\rho > 0$, $0 < f \leq 1$, and $r \geq 1$. Define*

$$\psi(\omega) := \frac{f}{\theta} \{ \lambda \rho^2 + \varphi \omega \rho \}, \quad (6-12)$$

and let $x^*(\omega)$ denote the unique, positive value of the healthy-cell density predicted by Theorem 5.1 and found by solving (6-10). Then there is a unique positive root of $\kappa_2 x^2 + \kappa_1(\omega)x + \psi(\omega) = 0$. Denote this root as $z(\omega)$. Then $0 < z(\omega) < x^*(\omega)$

and $0 < z'(\omega) < \infty$, $|z''(\omega)| < \infty$, and the sign of $z''(\omega)$ does not change and is equivalent to the sign of ζ , where

$$\zeta = \kappa_2(\psi' \kappa_1')^2 - \kappa_1(0)\psi' \kappa_1' + \psi(0). \tag{6-13}$$

Proof. The assumption that $R_0 > 1$ is equivalent to the inequality $\rho < 1 - \varphi\omega$. Thus, comparing ψ with κ_0 from (5-3c) shows that $0 < \psi(\omega) < \kappa_0(\omega)$. Therefore, since $\kappa_2 < 0$ (as was shown in the proof of Theorem 5.1), the equation $\kappa_2x^2 + \kappa_1(\omega)x + \psi(\omega) = 0$ has two real roots of opposite sign. Denoting the positive root as z , it follows that $0 < z(\omega) < x^*(\omega)$. Since κ_2 is independent of ω , differentiating both sides of $\kappa_2x^2 + \kappa_1(\omega)x + \psi(\omega) = 0$ yields

$$z'(\omega) = -\kappa_1'(\omega)z(\omega) + \psi'(\omega)2\kappa_2z(\omega) + \kappa_1(\omega). \tag{6-14}$$

Note that both $\kappa_1'(\omega)$ and $\psi'(\omega) > 0$ are independent of ω so the functional dependence on ω will be dropped for convenience. Since $\theta = 1 + p_2\varphi/q_2$ and $\rho = 1 - p_1/q_1$, (6-11) yields that κ_1' is positive if and only if $r + 1 > \rho + f\rho(1 - 2\lambda)$, which holds since $\lambda < 1$ and $r \geq 1$, $0 < \rho < 1$, $0 < f < 1$ by assumption. Since $\kappa_2 < 0$ and $z(\omega)$ is the positive root of the quadratic equation $\kappa_2x^2 + \kappa_1(\omega)x + \psi(\omega) = 0$, it follows that the denominator in (6-14) is negative and $0 < z(\omega) < x^*(\omega)$.

Differentiating $dz/d\omega$ from (6-14) yields that

$$z''(\omega) = \kappa_1'(\kappa_1'z(\omega) + \psi') - z'(\omega)(\kappa_1'\kappa_1(\omega) - 2\kappa_2\psi')(2\kappa_2z(\omega) + \kappa_1(\omega))^2.$$

This shows that $|z''(\omega)| < \infty$. We substitute $z'(\omega)$ from (6-14) to get that $z''(\omega)$ is positive if and only if

$$(\kappa_1'z(\omega) + \psi')\{\kappa_1' + \kappa_1'\kappa_1(\omega) - 2\kappa_2\psi'2\kappa_2z(\omega) + \kappa_1(\omega)\} > 0,$$

and using the conditions $\kappa_2 < 0$ and $\kappa_1'z(\omega) + \psi' > 0$, it follows that $z''(\omega)$ is positive if and only if

$$z(\omega) + \kappa_1(\omega)\kappa_2 - \psi' \kappa_1' = \kappa_1(\omega)2\kappa_2 - \sqrt{\kappa_1(\omega)^2 - 4\kappa_2\psi(\omega)2\kappa_2} - \psi' \kappa_1' > 0,$$

which is equivalent to

$$\kappa_2(\psi' \kappa_1')^2 - \kappa_1(\omega)\psi' \kappa_1' + \psi(\omega) > 0.$$

The first term is independent of ω and note that the derivative of the last two terms is zero so that the last two terms are also independent of ω . Since κ_1' and $\psi' = f\varphi\rho/\theta$ are positive, this inequality holds by the assumption (6-13). □

In order to prove local asymptotic stability of the disease equilibrium under certain parameter constraints, it will be necessary to use the properties of $z(\omega)$, $z'(\omega)$, and $z''(\omega)$ from Lemma 6.1.

Lemma 6.2. *Assume the hypotheses in Lemma 6.1 hold. Define the function $F(\omega)$ by*

$$F(\omega) := m z(\omega) + s(\omega), \quad \omega \in [0, \bar{\omega}], \quad (6-15)$$

where $\bar{\omega}$ is as in (5-9) and

$$m := 2r\theta - \rho(r + 1 - \rho)(1 + \theta), \quad s(\omega) := (r + 1 - \rho)(1 - \varphi\omega) - r\theta. \quad (6-16)$$

Then $F(\omega) \geq 0$ on $(0, \bar{\omega})$.

Proof. The constant m is positive if and only if

$$r > \rho\theta(1 - \rho) + 1 - \rho\theta(1 - \rho) + \theta - \rho,$$

which follows since $\theta > 1$ and $\rho < 1$. Therefore, since $s''(\omega) = 0$ and $F''(\omega) = m z''(\omega)$, we have $F''(\omega)$ is finite and has the same sign as ζ from (6-13). Since $R_0 = 1$ if and only if $\rho = 1 - \varphi\bar{\omega}$, comparing (5-3c) and (6-12) shows that $\psi(\bar{\omega}) = c(\bar{\omega})$ so that $z(\bar{\omega}) = x^*(\bar{\omega}) = 1$. Now use $\rho = 1 - \varphi\bar{\omega}$ to get

$$F(\bar{\omega}) = m + s(\bar{\omega}) = \theta(1 - \rho)(r - \rho) > 0.$$

Now $s(0) = 1 - \rho - r(\theta - 1)$ so that if $r(\theta - 1) \leq 1 - \rho$ and $s(0) \geq 0$, it follows directly that $F(0) > 0$ since $z(0) > 0$. Otherwise, consider the case where $r(\theta - 1) > 1 - \rho$ and $s(0) < 0$. Note that $F(0) > 0$ if and only if $z(0) > -s(0)/m$. Since $\kappa_2 < 0$, $\psi(\omega) > 0$, and $z(\omega)$ is the positive root of $\kappa_2 x^2 + \kappa_1(\omega)x + \psi(\omega) = 0$, it follows that $F(0) > 0$ whenever

$$\kappa_2(s(0)m)^2 - \kappa_1(0)s(0)m + \psi(0) > 0. \quad (6-17)$$

After substituting $1 - \rho = p_1/q_1$ in (5-3a), (5-3b) and (6-12), we get

$$\kappa_2 = -\rho\theta^{-1}(r\theta\lambda - 1 + \rho) - r(1 - \rho) + \psi(0), \quad \kappa_1(0) = \theta^{-1}(r\theta\lambda - 1 + \rho) - 2\rho\psi(0).$$

We substitute these expressions into (6-17) and multiply by θm^2 to get that $F(0) > 0$ if and only if

$$(\rho(r\theta\lambda - 1 + \rho) + r\theta(1 - \rho))s(0)^2 + m(r\theta\lambda - 1 + \rho)s(0) < \theta\psi(0)(s(0)^2 + 2\rho s(0)m + m^2). \quad (6-18)$$

Since $\rho < 1$, $m > 0$ and $s(0) < 0$, it follows that

$$s(0)^2 + 2\rho s(0)m + m^2 > (s(0) + m)^2 > 0,$$

and the right side of the inequality in (6-18) is positive. The left side is the product of $s(0)$ and

$$[\rho(r\theta\lambda - 1 + \rho) + r\theta(1 - \rho)]s(0) + m(r\theta\lambda - 1 + \rho),$$

so that (6-18) holds whenever this quantity is positive. After substituting $s(0)$, m , and $\theta - 1 = \theta\lambda$ and then simplifying, this becomes

$$\theta(1 - \rho)\{r^2(\theta - 1) - r[\rho(\theta - 1) - (1 - \rho)] + \rho(1 - \rho)\},$$

so that (6-18) holds whenever

$$r^2(\theta - 1) - r[\rho(\theta - 1) - (1 - \rho)] + \rho(1 - \rho) > 0. \quad (6-19)$$

The left side is a quadratic function of r and, after some algebra, its minimum value is computed as $-(\rho\theta - 1)^2/[4(\theta - 1)]$, so there are two real zeros for the left side. Therefore, since $r \geq 1$, the inequality (6-19) holds whenever the larger of these two roots is less than 1. Equivalently, when $r = 1$ the left side of (6-19) must be positive. We substitute $r = 1$ to get $(1 - \rho)(\theta - \rho) > 0$, which follows since $\rho < 1$ and $\theta > 1$. Therefore, (6-18) follows and $F(0) > 0$.

Next, it will be shown that $F(\omega)$ is nonnegative on the entire interval $(0, \bar{\omega})$. First assume $\zeta \leq 0$. Then by Lemma 6.2, it follows that $F(\omega)$ is either linear or concave down on $(0, \bar{\omega})$. Since $F(0) > 0$ and $F(\bar{\omega}) > 0$, it follows that $F(\omega)$ is positive on the entire interval. Next assume $\zeta > 0$ so that $F(\omega)$ is concave up on $(0, \bar{\omega})$. If $F'(0)$ and $F'(\bar{\omega})$ have the same sign, then $F(\omega)$ is either increasing or decreasing on $(0, \bar{\omega})$, which again implies that $F(\omega)$ is positive on the entire interval. If $F'(0)$ and $F'(\bar{\omega})$ have opposite signs, there must exist $\omega^* \in (0, \bar{\omega})$ for which $F'(\omega^*) = 0$ and $F(\omega^*)$ is a minimum. If $F(\omega^*) < 0$, there exist two values $\omega_1 \in (0, \bar{\omega})$ and $\omega_2 \in (0, \bar{\omega})$, where $\omega_1 \neq \omega_2$ and $F(\omega_1) = F(\omega_2) = 0$. The corresponding values of z are given by $-s(\omega_1)/m$ and $-s(\omega_2)/m$. After squaring $F(\omega)$, it follows that these zeros for $F(\omega)$ must also obey

$$m^2z(\omega)^2 + 2mz(\omega)s(\omega) + s(\omega)^2 = 0.$$

Since z obeys $\kappa_2z^2 + \kappa_1(\omega)z + \psi = 0$ and $z(\omega) = -s(\omega)/m$, this equation is equivalent to

$$\kappa_2s(\omega)^2 - m\kappa_1(\omega)s(\omega) + m^2\psi(\omega) = 0.$$

Here $\kappa_2 < 0$ and $m^2\psi > 0$ so that this equation has two real roots with opposite sign. Since $z(\omega)$ must be positive, this leads to a contradiction, and therefore $F(\omega) \geq 0$ on $(0, \bar{\omega})$. \square

The next theorem uses Lemma 6.2 to show the disease equilibrium of the reduced system is locally asymptotically stable.

Theorem 6.3. *Assume $R_0 > 1$, $\rho > 0$, $0 < f \leq 1$, and $r \geq 1$. Then the disease equilibrium for the reduced system (6-1a)–(6-1c) is locally asymptotically stable.*

Proof. First use $1 - \rho = p_1/q_1$ with (6-4) to see that $t_2 + (p_1/q_1)x^* = -y^*$ so that

$$a_3 = q_1y^*\{-t_1 - r\rho x^* + \rho f\varphi(\eta y^* + \omega) - \rho(1 - \rho)x^*\}, \quad (6-20)$$

after substituting t_3 from (6-5). It follows that $a_3 > 0$ if and only if

$$-t_1 > r\rho x^* + \rho(1 - \rho)x^* - \rho f\varphi(\eta y^* + \omega). \quad (6-21)$$

We substitute t_1 from (6-3) to get that (6-21) is equivalent to

$$r(2x^* - 1) + (r + 1 - \rho)(y^* - \rho x^*) + \rho f\varphi(\eta y^* + \omega) > 0. \quad (6-22)$$

Then, after substituting for y^* from (5-1) and rearranging terms, it follows that $a_3 > 0$ if and only if

$$mx^* + s(\omega) + \rho\theta f\varphi(\eta y^* + \omega) > 0, \quad (6-23)$$

with m and $s(\omega)$ defined in (6-16). Since $m > 0$ and $0 < z(\omega) < x^*$, it follows that a sufficient condition for (6-23) is that

$$F(\omega) + \rho\theta f\varphi(\eta y^* + \omega) > 0 \quad (6-24)$$

for all $\omega \in (0, \bar{\omega})$. Using Lemma 6.2, $F(\omega) \geq 0$ on $(0, \bar{\omega})$. Furthermore, the inequality $\rho\theta f\varphi(\eta y^* + \omega) > 0$ implies that (6-24) holds and $a_3 > 0$ on $(0, \bar{\omega})$.

To show that $a_1 > 0$ note that when (6-21) holds, this implies that $t_1 < 0$. Since $\rho < 1$, it is clear from (6-4) that $t_2 < 0$ and it follows by inspection of (6-6) that $a_1 > 0$. Finally, in order to show $a_1 a_2 > a_3$, start with the identity

$$\frac{a_3}{q_1} = a_2 + q_1(t_1 + t_2) + p_1 x^* + \left(\frac{p_1}{q_1}\right)t_1 x^* - \rho\left(\frac{p_1}{q_1}\right)x^* y^*,$$

which is easily verified by inspection of (6-7) and (6-8) and simple algebra. Thus,

$$a_2 > \frac{a_3}{q_1} - t_1\left(q_1 + \left(\frac{p_1}{q_1}\right)x^*\right) - q_1\left(t_2 + \left(\frac{p_1}{q_1}\right)x^*\right).$$

Now use the fact that $t_1 < 0$ and $t_2 + (p_1/q_1)x^* = -y^*$ to see that

$$a_1 > q_1 \quad \text{and} \quad a_2 > \frac{a_3}{q_1},$$

which shows that $a_1 a_2 > a_3$. The Routh–Hurwitz conditions (6-9) hold, and the disease-free equilibrium (x^*, y^*, α^*) is locally asymptotically stable. \square

In certain parameter ranges, the reduced model may inform the full model (3-4a)–(3-4d). The Jacobian evaluated at the disease equilibrium for the full model is

$$J(x^*, y^*, v^*, \alpha^*) = \begin{bmatrix} t_1 & t_3 & -x^* & f\varphi y^* \\ -\rho y^* & t_2 & x^* & -\varphi y^* \\ 0 & p_1 & -q_1 & 0 \\ 0 & p_2 & 0 & -q_2 \end{bmatrix}. \quad (6-25)$$

In general, the eigenvalues of the reduced model determined from (6-2) cannot be used to determine the eigenvalues of (6-25). However, as discussed at the beginning

of this section, the time courses for x , y , and v in the reduced model (6-1a)–(6-1c) approximate these same time courses in the full model when φ is small and it is easily seen from (6-2) and (6-25) that as $\varphi \rightarrow 0$, the eigenvalues for the full model are given by the three eigenvalues of (6-2) and a fourth eigenvalue equal to $-q_2 < 0$. These eigenvalues depend continuously on φ and this suggests that [Theorem 6.3](#) should also hold for the full model when φ is small. A full analysis of the full model will not be presented here.

7. Conclusions

In this paper a new model of viral dynamics is presented in [Section 2](#). These equations are given by (2-1a)–(2-1d). The healthy- and unhealthy-cell growth dynamics are logistic. In addition, this model includes both immune response behavior and the noncytolytic mediated curing of infected cells. The main parameter values are obtained from the literature and presented in [Table 1](#). Simulations using these parameter values show that the model exhibits a range of typical behaviors including constant solutions as in [Figure 1](#) and periodicity as in [Figure 2](#). In [Section 3](#), the model equations are nondimensionalized. The basic reproduction ratio R_0 is computed in [Section 4](#) and defined in (4-4). Simulations in [Figure 3](#) show how healthy and unhealthy-cell densities depend on R_0 and it is shown that a necessary and sufficient condition that the disease-free equilibrium E_f is locally asymptotically stable is that $R_0 < 1$. The disease equilibrium E_d is computed in [Section 5](#) and [Figures 4](#) and [5](#) illustrate that there may be critical parameter values for which E_d bifurcates from a unique positive value to two positive values. For the parameter values used in these figures it can also be seen that the unique disease equilibrium is locally asymptotically stable and in the case of nonuniqueness, the smaller equilibrium is unstable, while the larger equilibrium is locally asymptotically stable. In [Section 6](#) a reduced system is analyzed by considering the immune response variable α to be at its steady-state value and eliminating the equation for α in the full model. This reduced system approximates the full model when the cytolytic clearance rate b or the ratio c/d of CTL response rate to CTL death rate is small. The Routh–Hurwitz conditions are then used to determine parameter values that guarantee a unique, locally asymptotically stable disease equilibrium in this reduced system.

The basic reproduction ratio can be used to understand how the parameters influence the disease state. Substituting dimensional parameters from (3-2) and (3-3) into (4-4) yields

$$R_0 = \frac{\beta K \gamma d}{\mu b I_0}.$$

Thus, R_0 decreases with bI_0/d . This ratio controls the effects of the immune response dynamics. In particular, increasing the rate at which the cytolytic immune

response occurs, b , or the basal level of immune response cells, I_0/d , decreases the total density of unhealthy hepatocytes, Y , and increases the total density of healthy hepatocytes, X . When the healthy-cell infection rate β is relatively large, as in [Figure 5](#), noncytolytic response controlled by the scaling parameter f in (2-1a) is more significant than cytolytic response b . On the other hand when β is relatively small as in [Figure 6](#), healthy cells remain near carrying capacity for all values of f , but increase rapidly with the cytolytic clearance rate. Thus these simulations suggests that the healthy-cell infection rate may play a significant role in the effectiveness of cytolytic vs. noncytolytic immune response.

The results presented here provide only a partial analysis of the model (2-1a)–(2-1d). For example, only local asymptotic stability is considered and neither the nonunique disease equilibrium nor periodic behavior (as in [Figure 2](#)) have been investigated in detail. Thus future work should include examining global stability of E_f , analyzing local asymptotic and global stability of E_d in the full system (2-1a)–(2-1d), and further investigations of the limit cycle behavior.

Acknowledgements

The authors would like to acknowledge Sam Houston State University's College of Science and Engineering Technology for its support and funding for an undergraduate research project which led to this manuscript.

References

- [Allen 2007] L. J. S. Allen, *Introduction to mathematical biology*, Pearson, Upper Saddle River, NJ, 2007.
- [Ciupe et al. 2007] S. M. Ciupe, R. M. Ribeiro, P. W. Nelson, G. Dusheiko, and A. S. Perelson, “The role of cells refractory to productive infection in acute hepatitis B viral dynamics”, *Proc. Natl. Acad. Sci. USA* **104**:12 (2007), 5050–5055.
- [Diekmann et al. 1990] O. Diekmann, J. A. P. Heesterbeek, and J. A. J. Metz, “On the definition and the computation of the basic reproduction ratio R_0 in models for infectious diseases in heterogeneous populations”, *J. Math. Biol.* **28**:4 (1990), 365–382. [MR](#) [Zbl](#)
- [Edelstein-Keshet 1988] L. Edelstein-Keshet, *Mathematical models in biology*, Random House, New York, 1988. [MR](#) [Zbl](#)
- [Hews et al. 2010] S. Hews, S. Eikenberry, J. D. Nagy, and Y. Kuang, “Rich dynamics of a hepatitis B viral infection model with logistic hepatocyte growth”, *J. Math. Biol.* **60**:4 (2010), 573–590. [MR](#) [Zbl](#)
- [Kim et al. 2012] H. Y. Kim, H.-D. Kwon, T. S. Jang, J. Lim, and H.-S. Lee, “Mathematical modeling of triphasic viral dynamics in patients with HBeAg-positive chronic hepatitis B showing response to 24-week clevudine therapy”, *PLoS ONE* **7**:11 (2012), art. id. e50377.
- [Lavanchy 2004] D. Lavanchy, “Hepatitis B virus epidemiology, disease burden, treatment, and current and emerging prevention and control measures”, *J. Viral Hepatitis* **11**:2 (2004), 97–107.

- [Locarnini et al. 2015] S. Locarnini, A. Hatzakis, D. S. Chen, and A. Lok, “Strategies to control hepatitis B: public policy, epidemiology, vaccine and drugs”, *J. Hepatology* **62**:1, Suppl. (2015), S76–S86.
- [Nowak and Bangham 1996] M. A. Nowak and C. R. M. Bangham, “Population dynamics of immune responses to persistent viruses”, *Science* **272**:5258 (1996), 74–79.
- [Nowak et al. 1996] M. A. Nowak, S. Bonhoeffer, A. M. Hill, R. Boehme, H. C. Thomas, and H. McDade, “Viral dynamics in hepatitis B virus infection”, *Proc. Natl. Acad. Sci. USA* **93**:9 (1996), 4398–4402.
- [Pang et al. 2012] J. Pang, J.-a. Cui, and J. Hui, “The importance of immune responses in a model of hepatitis B virus”, *Nonlinear Dynam.* **67**:1 (2012), 723–734. MR Zbl
- [Perelson 2002] A. S. Perelson, “Modelling viral and immune system dynamics”, *Nature Rev. Immunology* **2** (2002), 28–36.
- [Rodriguez et al. 2017] A. C. Rodriguez, M. Chung, and S. M. Ciupe, “Understanding the complex patterns observed during hepatitis B virus therapy”, *Viruses* **9**:5 (2017), art. id. 117.
- [Stanaway et al. 2016] J. D. Stanaway, A. D. Flaxman, M. Naghavi, C. Fitzmaurice, T. Vos, I. Abubakar, L. J. Abu-Raddad, R. Assadi, N. Bhala, B. Cowie, M. H. Forouzanfour, J. Groeger, K. M. Hanafiah, K. H. Jacobsen, S. L. James, J. MacLachlan, R. Malekzadeh, N. K. Martin, and G. S. Cooke, “The global burden of viral hepatitis from 1990 to 2013: findings from the Global Burden of Disease Study 2013”, *The Lancet* **388**:10049 (2016), 1081–1088.
- [Thieme 2003] H. R. Thieme, *Mathematics in population biology*, Princeton University Press, 2003. MR Zbl
- [Vargas-De-León 2014] C. Vargas-De-León, “Global properties for a virus dynamics model with lytic and non-lytic immune responses, and nonlinear immune attack rates”, *J. Biol. Systems* **22**:3 (2014), 449–462. MR Zbl
- [Wodarza et al. 2002] D. Wodarza, J. P. Christensen, and A. R. Thomsen, “The importance of lytic and nonlytic immune responses in viral infections”, *Trends in Immunology* **23**:4 (2002), 194–200.
- [Zapata et al. 2014] H. D. T. Zapata, A. G. C. Casso, D. Bichara, and S. Lee, “Role of active and inactive cytotoxic immune response in human immunodeficiency virus dynamics”, *Osong Pub. Health Res. Perspect.* **5**:1 (2014), 3–8.

Received: 2019-10-26

Revised: 2020-03-12

Accepted: 2020-03-14

jga001@shsu.edu

Department of Mathematics and Statistics,
Sam Houston State University, Huntsville, TX, United States

smccoy10@vols.utk.edu

Department of Mathematics, University of Tennessee,
Knoxville, TN, United States

INVOLVE YOUR STUDENTS IN RESEARCH

Involve showcases and encourages high-quality mathematical research involving students from all academic levels. The editorial board consists of mathematical scientists committed to nurturing student participation in research. Bridging the gap between the extremes of purely undergraduate research journals and mainstream research journals, *Involve* provides a venue to mathematicians wishing to encourage the creative involvement of students.

MANAGING EDITOR

Kenneth S. Berenhaut Wake Forest University, USA

BOARD OF EDITORS

Colin Adams	Williams College, USA	Robert B. Lund	Clemson University, USA
Arthur T. Benjamin	Harvey Mudd College, USA	Gaven J. Martin	Massey University, New Zealand
Martin Bohner	Missouri U of Science and Technology, USA	Mary Meyer	Colorado State University, USA
Amarjit S. Budhiraja	U of N Carolina, Chapel Hill, USA	Frank Morgan	Williams College, USA
Pietro Cerone	La Trobe University, Australia	Mohammad Sal Moslehian	Ferdowsi University of Mashhad, Iran
Scott Chapman	Sam Houston State University, USA	Zuhair Nashed	University of Central Florida, USA
Joshua N. Cooper	University of South Carolina, USA	Ken Ono	Univ. of Virginia, Charlottesville
Jem N. Corcoran	University of Colorado, USA	Yuval Peres	Microsoft Research, USA
Toka Diagana	University of Alabama in Huntsville, USA	Y.-F. S. Pétermann	Université de Genève, Switzerland
Michael Dorff	Brigham Young University, USA	Jonathon Peterson	Purdue University, USA
Sever S. Dragomir	Victoria University, Australia	Robert J. Plemmons	Wake Forest University, USA
Joel Foisy	SUNY Potsdam, USA	Carl B. Pomerance	Dartmouth College, USA
Erin W. Fulp	Wake Forest University, USA	Vadim Ponomarenko	San Diego State University, USA
Joseph Gallian	University of Minnesota Duluth, USA	Bjorn Poonen	UC Berkeley, USA
Stephan R. Garcia	Pomona College, USA	József H. Przytycki	George Washington University, USA
Anant Godbole	East Tennessee State University, USA	Richard Rebarber	University of Nebraska, USA
Ron Gould	Emory University, USA	Robert W. Robinson	University of Georgia, USA
Sat Gupta	U of North Carolina, Greensboro, USA	Javier Rojo	Oregon State University, USA
Jim Haglund	University of Pennsylvania, USA	Filip Saidak	U of North Carolina, Greensboro, USA
Johnny Henderson	Baylor University, USA	Hari Mohan Srivastava	University of Victoria, Canada
Glenn H. Hurlbert	Virginia Commonwealth University, USA	Andrew J. Sterge	Honorary Editor
Charles R. Johnson	College of William and Mary, USA	Ann Trenk	Wellesley College, USA
K. B. Kulasekera	Clemson University, USA	Ravi Vakil	Stanford University, USA
Gerry Ladas	University of Rhode Island, USA	Antonia Vecchio	Consiglio Nazionale delle Ricerche, Italy
David Larson	Texas A&M University, USA	John C. Wierman	Johns Hopkins University, USA
Suzanne Lenhart	University of Tennessee, USA	Michael E. Zieve	University of Michigan, USA
Chi-Kwong Li	College of William and Mary, USA		

PRODUCTION

Silvio Levy, Scientific Editor

Cover: Alex Scorpan

See inside back cover or msp.org/involve for submission instructions. The subscription price for 2020 is US \$205/year for the electronic version, and \$275/year (+\$35, if shipping outside the US) for print and electronic. Subscriptions, requests for back issues and changes of subscriber address should be sent to MSP.

Involve (ISSN 1944-4184 electronic, 1944-4176 printed) at Mathematical Sciences Publishers, 798 Evans Hall #3840, c/o University of California, Berkeley, CA 94720-3840, is published continuously online. Periodical rate postage paid at Berkeley, CA 94704, and additional mailing offices.

Involve peer review and production are managed by EditFlow[®] from Mathematical Sciences Publishers.

PUBLISHED BY

 **mathematical sciences publishers**

nonprofit scientific publishing

<http://msp.org/>

© 2020 Mathematical Sciences Publishers

Hyperbolic triangular prisms with one ideal vertex	361
GRANT S. LAKELAND AND CORINNE G. ROTH	
On the sandpile group of Eulerian series-parallel graphs	381
KYLE WEISHAAR AND JAMES SEIBERT	
Linkages of calcium-induced calcium release in a cardiomyocyte simulated by a system of seven coupled partial differential equations	399
GERSON C. KROIZ, CARLOS BARAJAS, MATTHIAS K. GOBBERT AND BRADFORD E. PEERCY	
Covering numbers and schlicht functions	425
PHILIPPE DROUIN AND THOMAS RANSFORD	
Uniqueness of a three-dimensional stochastic differential equation	433
CARL MUELLER AND GIANG TRUONG	
Sharp sectional curvature bounds and a new proof of the spectral theorem	445
MAXINE CALLE AND COREY DUNN	
Qualitative investigation of cytolytic and noncytolytic immune response in an HBV model	455
JOHN G. ALFORD AND STEPHEN A. MCCOY	
A Cheeger inequality for graphs based on a reflection principle	475
EDWARD GELERNT, DIANA HALIKIAS, CHARLES KENNEY AND NICHOLAS F. MARSHALL	
Sets in \mathbb{R}^d determining k taxicab distances	487
VAJRESH BALAJI, OLIVIA EDWARDS, ANNE MARIE LOFTIN, SOLOMON MCHARO, LO PHILLIPS, ALEX RICE AND BINEYAM TSEGAYE	
Total difference chromatic numbers of graphs	511
RANJAN ROHATGI AND YUFEI ZHANG	
Decline of pollinators and attractiveness of the plants	529
LEILA ALICKOVIC, CHANG-HEE BAE, WILLIAM MAI, JAN RYCHTÁŘ AND DEWEY TAYLOR	